Chapter

Frequency Reconfigurable UWB Antenna Design for Wireless Applications

Ritesh Kumar Saraswat and Mithilesh Kumar

Abstract

A frequency band reconfigurable antenna is designed and experimentally analyzed. Proposed design achieve UWB (3.1–10.6 GHz), two dual band and two narrow band switching states by implementation of PIN diodes inside the slotted ground. Antenna covers the various wireless standards WLAN, WiMAX, WiFi and UWB with return loss $S_{11} < -10$ dB. Proposed antenna is also operating at 9.2 GHz to include the airborne radar applications. Simulated and experimental results are compared and found to be in good agreement.

Keywords: cognitive radio (CR), frequency-band reconfigurable, RF switch p-i-n diode, ultra wideband (UWB) antenna, WLAN

1. Introduction

Present scenario of wireless communication system required compact and multiple band antenna design. Since many systems are operating at multiple frequency range, requiring dual and triple band antenna for various applications such as WLAN, WiMAX, RFID, satellite communication, etc. Presently, many printed monopole antenna are proposed. Serve for wireless applications to cover the wireless standards for Wireless local area network (WLAN: 2.4–2.48, 5.15–5.35, and 5.75–5.825 GHz) and worldwide interoperability for microwave access (WiMAX: 3.4–3.69 GHz) are two among the available wireless standards which allow interconnections of devices for communication. To achieve multi-functionality, various parameters of antenna such as polarization characteristics, resonant frequency, patterns and impedance bandwidth etc., are reconfigured as per requirements [1].

Presently wireless communication systems are adopting the concept of cognitive radio system where using a sensing antenna performing the monitoring of the spectrum, and can be reconfigured to operate over a desired frequency band. This system is required a frequency band reconfigurable antenna as a sensing element [2]. Most of frequency band reconfigurable antennas providing the band switching between narrowband modes [3–5].

Antenna obtained the quad-band switching by implementation of microelectromechanical systems (MEMS) switch [3]. Another frequency band reconfigurable patch antenna is proposed that operate in four different modes with the help of switching elements [4]. Recently, many microstip patch antenna have been designed that indicate the switching facility in narrowband as well as wideband modes [6–11]. In [6], a Vivaldi antenna is designed that provide the wideband and

narrowband mode switching facility. A frequency band reconfigurable antenna with four photoconductive switches is proposed that operating with switching between the three narrowband modes and UWB mode [7]. In [9], antenna has been proposed with narrowband and wideband functionality with reconfigurability characteristics is achieved with the implementation of p-i-n and varactor diodes. Tunable EBG structure are analyzed with active switching devices FET and obtained the transmission characteristics of the structure [12, 13]. Many techniques such as defective ground [14], etching slots [15, 16], metamaterial loading [17–23], dielectric resonator [24], fractal geometry [25, 26], etc., are applied to accomplish multiband reconfigurable operation to cover various wireless applications.

In this chapter, firstly design the octagonal shape patch antenna and implementing the inverted L shaped switchable slotted ground yielded switchable resonant modes such as, two narrowband modes (5.05–5.89 and 8.76–9.80 GHz), two dual band modes (2.21–2.52 GHz and 5.07–5.89 GHz and 2.18–2.52 GHz and 8.78–9.71 GHz) and UWB mode (2.87–16.56 GHz) for wireless applications. As per requirement to design antenna to frequency band reconfigurability introducing the five switching elements p-i-n diodes placed inside the slotted ground. The proposed design is compact in size as compared to antennas are discussed in published literature [6–11]. The simulation work of antenna is done by using CST Microwave Studio (CST MWS) software [27] and measurement is performed with the help of VNA (vector network analyzer-E5071C (300 KHz–20 GHz) ENA series Agilent Technologies). The fabrication of proposed structure is executed by using of PCB prototype machine (Caddo-71).

Following sections focused on the antenna designing with parametric study and switchable modes analysis with results in simulated as well as measurement modes.

2. Ultra wideband (UWB) antenna design

In this section initially octagonal shape monopole antenna size of 40 × 40 × 0.40 mm^3 is designed, as represented in configuration "a" of **Figure 1**. The proposed design is constructed on 0.40 mm thick Roger RT 5880 substrate with the relative permittivity 2.2, fed with 50 ohm microstrip feed line. Octagonal shape radiating element has the dimensions ab = ef = 10 mm, bc = ha = 5.14 mm, cd = gh = 6.0 mm and de = fg = 5.14 mm attached with feedline of dimensions 22 × 1.25 × 0.01 mm^3. On back side of antenna, ground plane

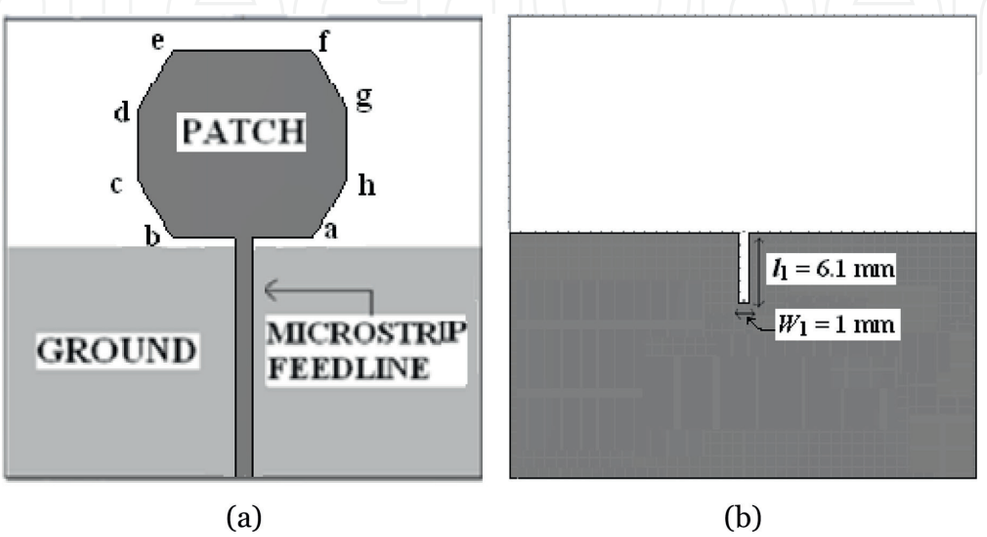

Figure 1.
Configuration of the UWB antenna: (a) front view of structure and (b) back view of structure.

exist with length of 21.1 mm, width of 40 mm and thickness of 0.01 mm. **Figure 1** shows the configuration of the proposed antenna with a top view and bottom view.

The operational performance of the antenna is analyzed with variations in its parameters such as ground slot dimensions (length l_1 and width W_1) are known as the parametric study of the proposed design. This study is carried out by variations in slot length l_1 and width W_1 while keeping other parameters constant. Slot length l_1 and width W_1 is varied from 0 to 7 mm and 0.6 to 1.4 mm respectively, as depicted in **Figure 2**. It is observed that, as variation are done in the value of l_1 and W_1, the reflection coefficient (S_{11}) is changes and the respective frequency band is also changes accordingly. The optimized impedance matching for UWB band characteristics is achieved at length l_1 = 6.1 mm and width W_1 = 1 mm.

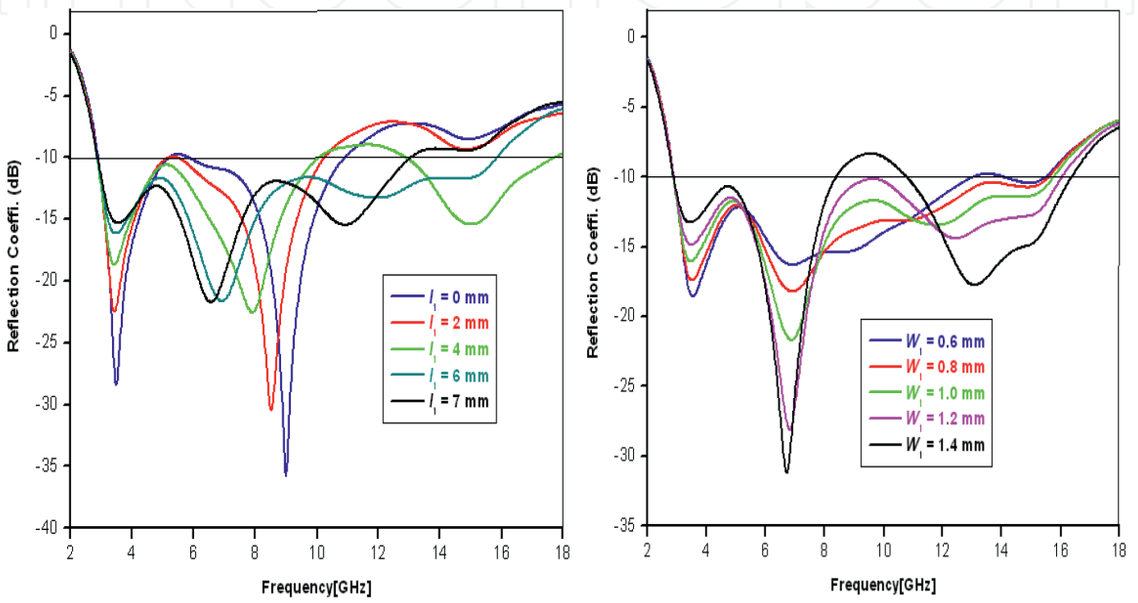

Figure 2.
Simulated reflection coefficient S_{11} of the proposed antenna for different values of l_1 and W_1.

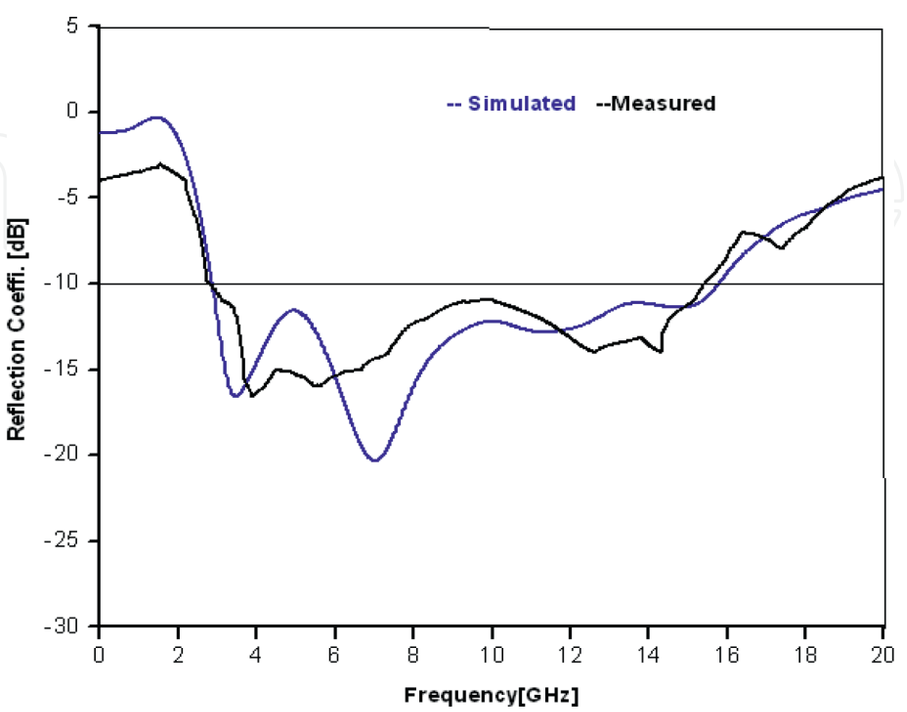

Figure 3.
Simulated and measured reflection coefficient S_{11} of the proposed UWB antenna.

From **Figure 2**, it is indicated that at lower frequencies (2–4 GHz) that the impedance matching is improved when the slot dimensions are reduced (either by reducing l_1 or W_1). At higher frequencies (above 5 GHz), the impedance matching is enhanced when the slot dimensions are increased. The input reflection coefficient S_{11} (below −10 dB) of UWB antenna is achieved at the optimized value of l_1 = 6.1 mm and W_1 = 1 mm. The impedance bandwidth of 141% (2.87–16.56 GHz) under simulation and 140% (2.85–15.85 GHz) in measurement is obtained as shown in **Figure 3**.

3. Narrowband and dual band antenna design

The UWB monopole antenna can be reconfigured to others frequency bands by using an inverted L and rectangular shaped slotted structure placed on the ground plane, as shown in **Figure 4**. This inverted L-shaped slot in ground plane generating an additional current path due to the perturbation of the current flow in antenna structure that leads to the filter characteristics, responsible to suppress the frequencies outside the desired frequency band. These ground slots are generating the stop bands in the UWB frequency range [9]. **Figure 5** represents the different filter structures of the proposed design by variation in the inverted L-shaped slot.

Figure 6 represents the input reflection coefficient S_{11} (below −10 dB) of the antenna for different filter structures. Structure I and II are creating the dual bands whereas structure III and IV are responsible for obtaining the single bands only.

Moreover, the bandwidth of each filtering structure in **Figure 6**, is controllable with changing the length l_2 and width W_2 of parallel vertical arms (in **Figure 4**). By the variations of these arms dimensions impedance bandwidth changes accordingly, as shown in **Figure 7**. While increasing the slot length l_2 and width W_2,

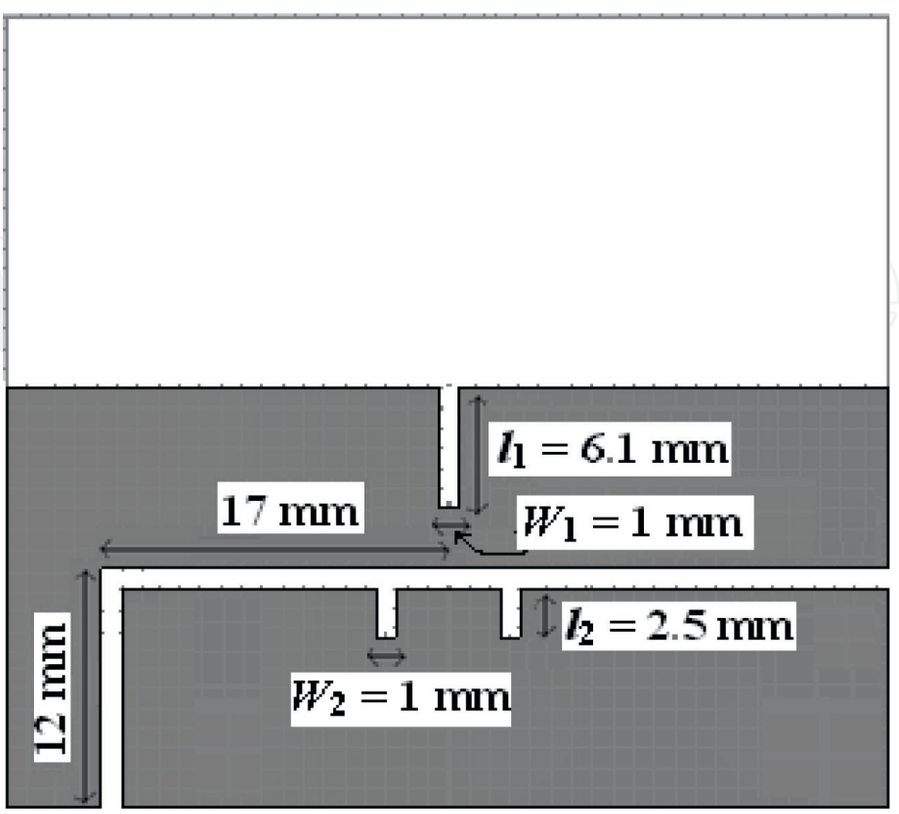

Figure 4.
Slotted structure on ground plane.

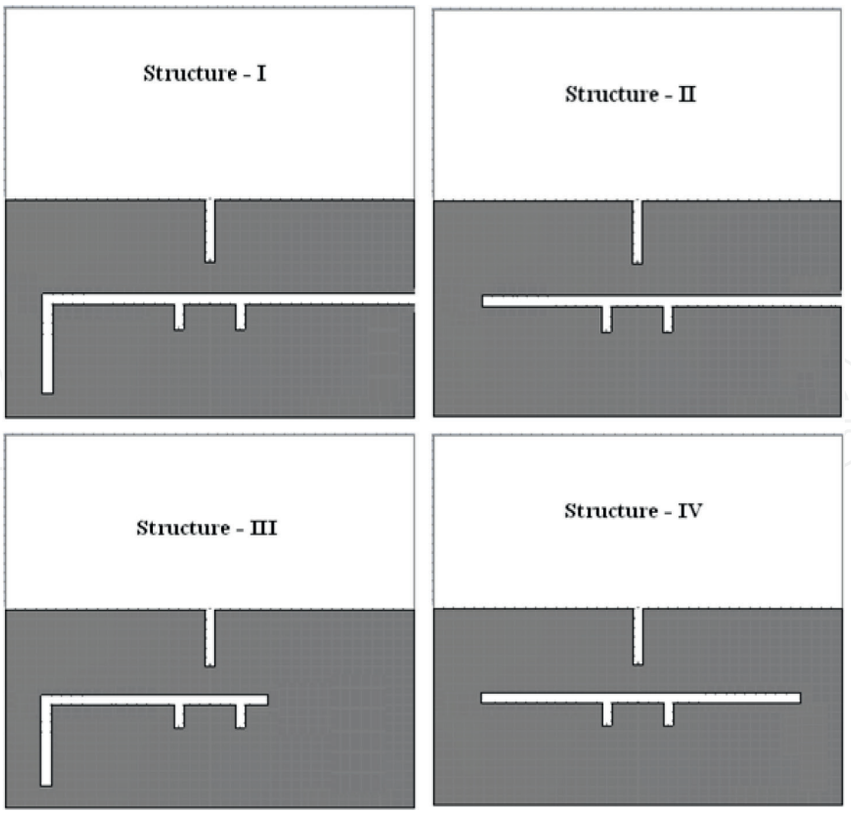

Figure 5.
Filter structures placed on the ground plane.

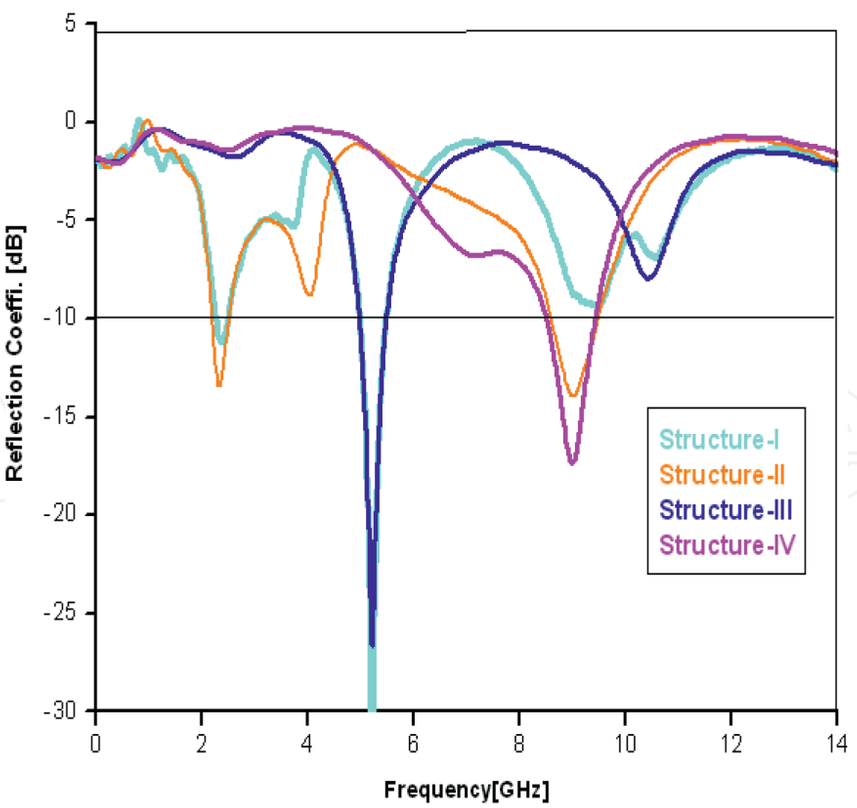

Figure 6.
Simulated reflection coefficient S_{11} of the antenna for filter structures in **Figure 5**.

the bandwidth of antenna decreases from 30 to 12% in structure III. The desired resonant band with the input reflection coefficient S_{11} (below −10 dB) is achieved at the optimized value l_2 = 2.5 mm and W_2 = 1 mm respectively.

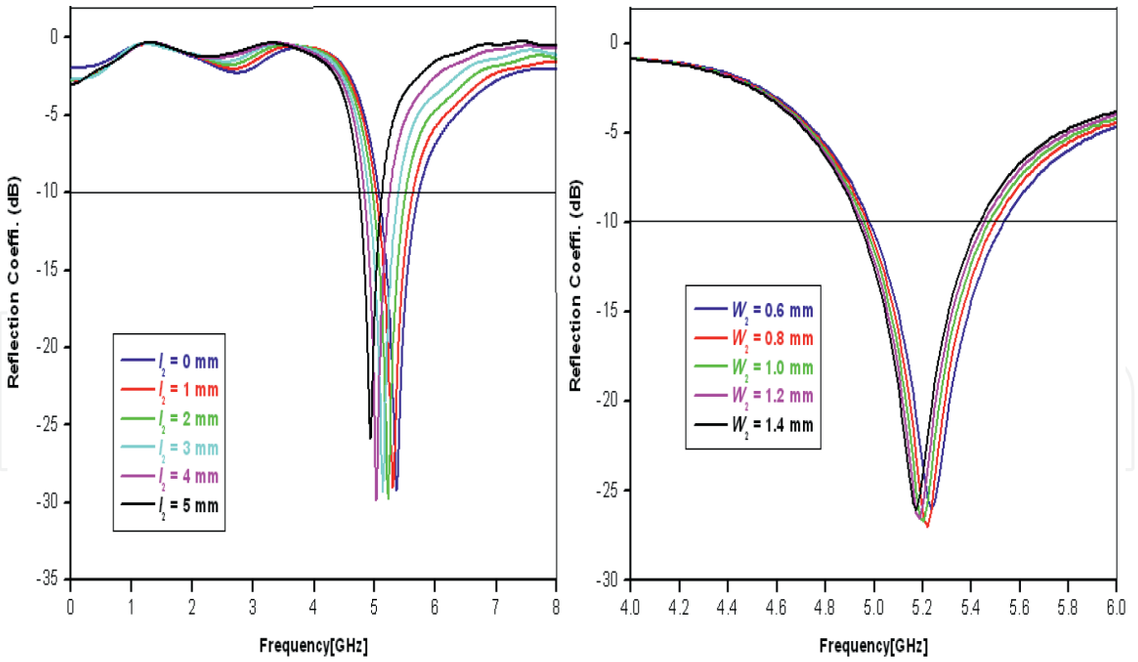

Figure 7.
Simulated reflection coefficient S_{11} of the antenna for different values of l_2 and W_2 in structure-III.

4. Frequency reconfigurable antenna design

In this section analyzed the reconfiguration of UWB mode of proposed design to another narrowband and dual band modes. This reconfiguration is done by implementation of filter structures on the ground plane by placing of five switching elements p-i-n diodes inside it, as indicated in **Figure 8**. The switches D_1–D_5 are positioned in such a way to obtain the required structures I–IV for desired frequency bands. If diode D_1 is on and remaining are off, we will get a filter structure like structure-I for dual band.

For biasing of p-i-n diodes, apply the dc voltage across the p-i-n diodes with the help of metal strips dimension of 2 × 0.6 mm^2, as indicated in **Figure 8**. As shown in **Figure 8**, blocking capacitor of 100 pF is also connected with diode, to provide the isolation between the dc and the RF signal. A beam lead p-i-n diodes (ALPHA-6355) are placed inside the ground slot, where 0.7 V dc is required for biasing of diode. During ON state (forward bias) of diode, it exhibit resistance of 2.6 ohm while in case of OFF state (reverse bias) it represents 0.081 pF [28].

Figure 9 shows the electrical equivalent circuit of the diode for both states (ON/OFF state). For On state, it represents a series combination of fixed inductor (L_s) and a current-controlled resistor (R_s), whereas for OFF state, it indicates a shunt combination of intrinsic-layer capacitance (C_p) and the resistance (R_s) in series with fixed inductance (L_s). The intrinsic-layer capacitance (C_p) is a combination of the stray capacitance C_s and the junction's capacitance C_j.

As per **Table 1**, narrow bands, dual bands and UWB band are obtained by changing the states of diodes and compare the frequency bands and 10-dB bandwidth in simulation and measurement mode. The proposed antenna is initially simulated with the help of simulation software CST Microwave Studio (MWS) [27] and thereafter, fabricated on FR4 substrate with optimized values. **Figure 10** shows the fabricated prototype of the proposed antenna.

A setup is used for frequency band reconfigurable structure to observe the measured reflection coefficient (S_{11}) with the help of vector network analyzer (VNA) and radiation characteristics by using anechoic chamber, shown in **Figure 11**.

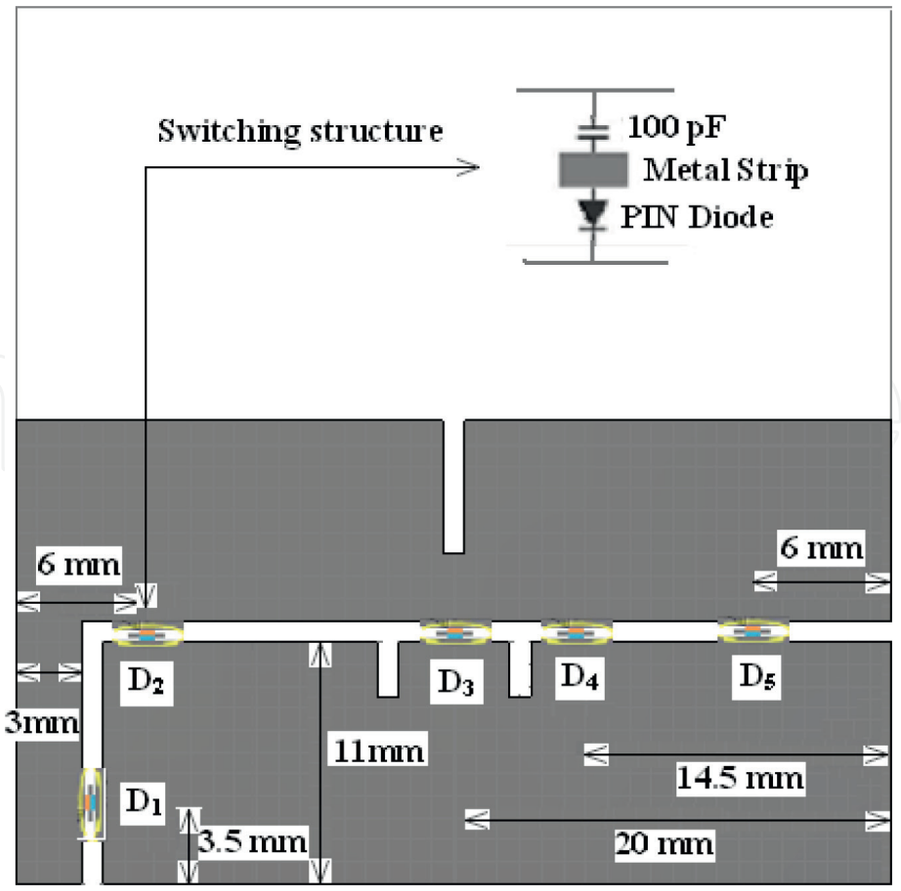

Figure 8.
Switchable filter structure on the ground plane (unit: millimeters).

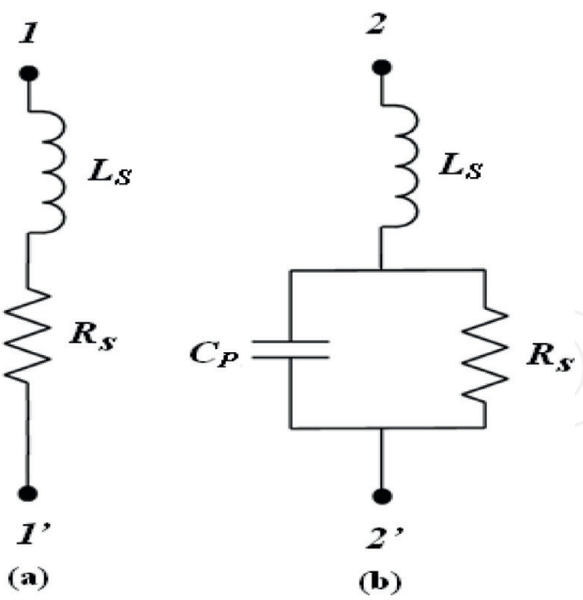

Figure 9.
Equivalent circuit for p-i-n diode: (a) ON-state (forward bias) and (b) OFF-state (reverse bias).

The simulated and measured reflection coefficients S_{11} for all five states are shown in **Figure 12**. Comparison of simulated S_{11} with measured ones is indicated as a good agreement between them. From **Table 1**, for narrowband states I achieve the bandwidth of 16% (5.05–5.89 GHz) and 14% (5.01–5.79 GHz) in simulation and measurement mode respectively. For state II (narrowband), obtained bandwidth of 11% (8.76–9.80 GHz) and 10% (8.68–9.69 GHz) in simulation and measurement

Diode	D_1	D_2	D_3	D_4	D_5	Frequency bands (in GHz)		10-dB bandwidth (%)		Characteristics
States						Simulated	Measured	Simulated	Measured	
I	ON	OFF	OFF	ON	OFF	5.05–5.91	5.01–5.79	16	14	Narrow band
II	OFF	ON	OFF	OFF	ON	8.76–9.80	8.68–9.69	11	10	Narrow band
III	ON	OFF	OFF	OFF	OFF	2.21–2.52 and 5.07–5.89	2.20–2.50 and 5.05–5.90	13 and 15	12 and 15	Dual band
IV	OFF	ON	OFF	OFF	OFF	2.18–2.52 and 8.78–9.71	2.19–2.50 and 8.70–9.60	14 and 10	13 and 9	Dual band
V	ON	ON	ON	ON	ON	2.87–16.56	2.85–15.85	141	140	UWB

Table 1.
Details of combinations of p-i-n diodes with simulated and measured frequency band and bandwidth in each states.

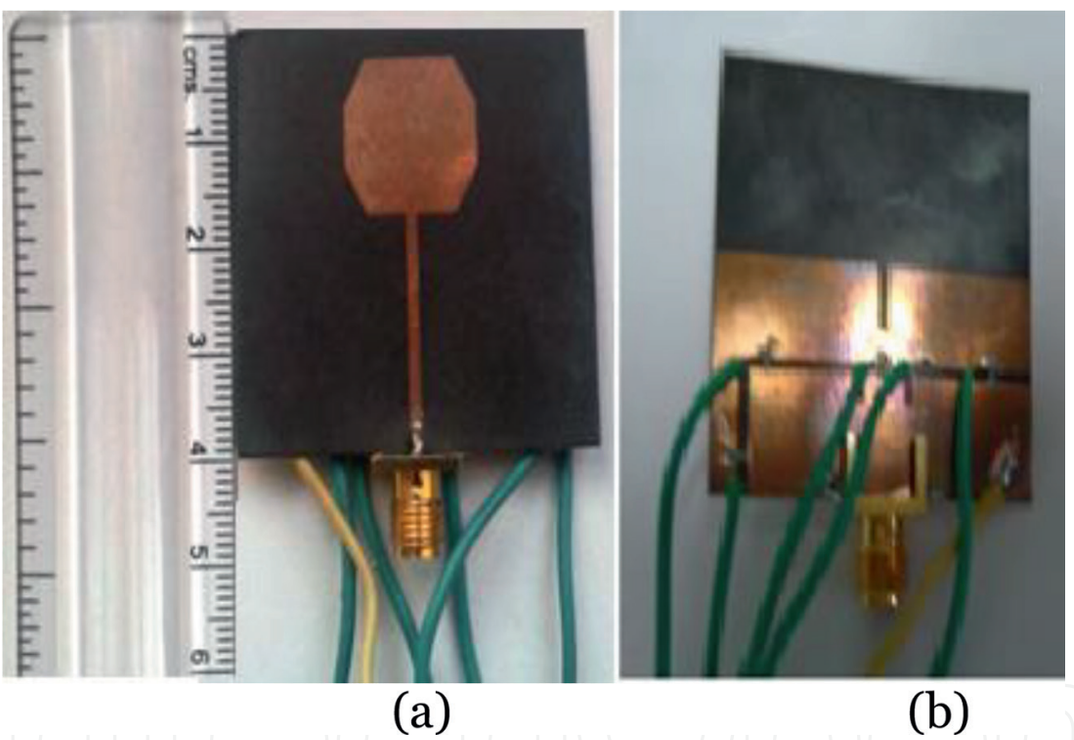

Figure 10.
Images of the fabricated antenna: (a) top view and (b) bottom view.

mode respectively. For next state III, antenna resonant in dual band mode and achieve impedance bandwidth of 13% (2.21–2.52 GHz) and 15% (5.07–5.89 GHz) under simulation and 12% (2.20–2.50 GHz) and 15% (5.05–5.90 GHz) during measurement. For State IV, antenna identifies the operating bandwidth of 14% (2.18–2.52 GHz) and 10% (8.78–9.71 GHz) and 13% (2.19–2.50 GHz) and 9% (8.70–9.60 GHz) during simulation and measurement mode respectively. For V state of UWB mode, antenna indicates the operating bandwidth of 141% (2.87–16.87 GHz) and 140% (2.97–16.80 GHz) under simulation and measurement mode respectively.

The resonant bands are achieved by switching states of diodes can serve several wireless applications such as WLAN, WiMAX, WiFi and UWB. As per IEEE standards the WLAN is identify for 802.11b/g/n (2.4–2.48 GHz), 802.11a/h/j/n (5.2 GHz) and ISM band (2.4–2.5 GHz). Wireless standards WiMAX, WiFi and UWB are identify for frequency bands of 2.3–2.4 and 5.15–5.85 GHz, 2.40–2.48

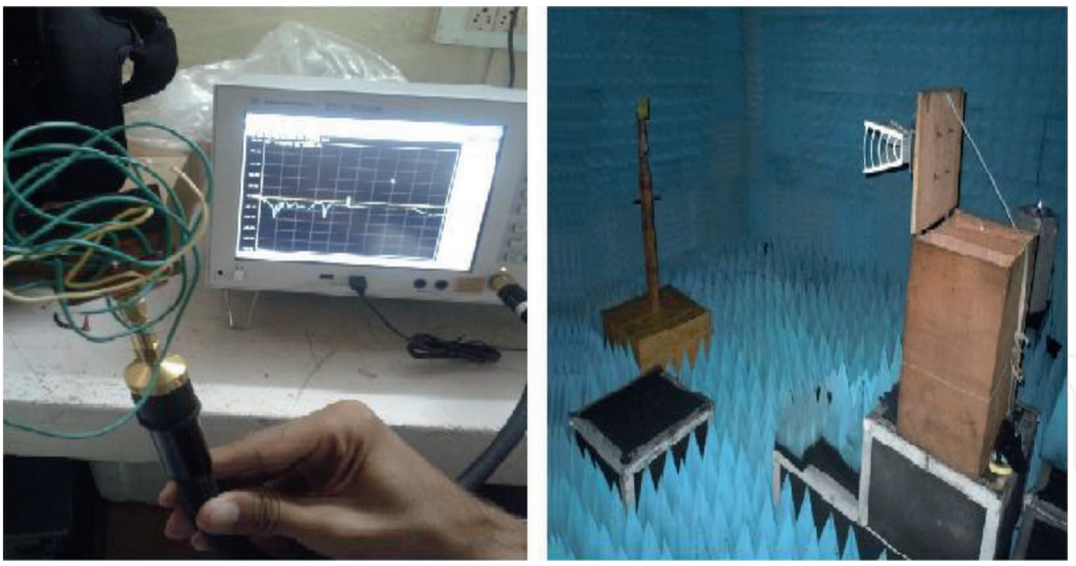

Figure 11.
Images of measurement setup for proposed antenna.

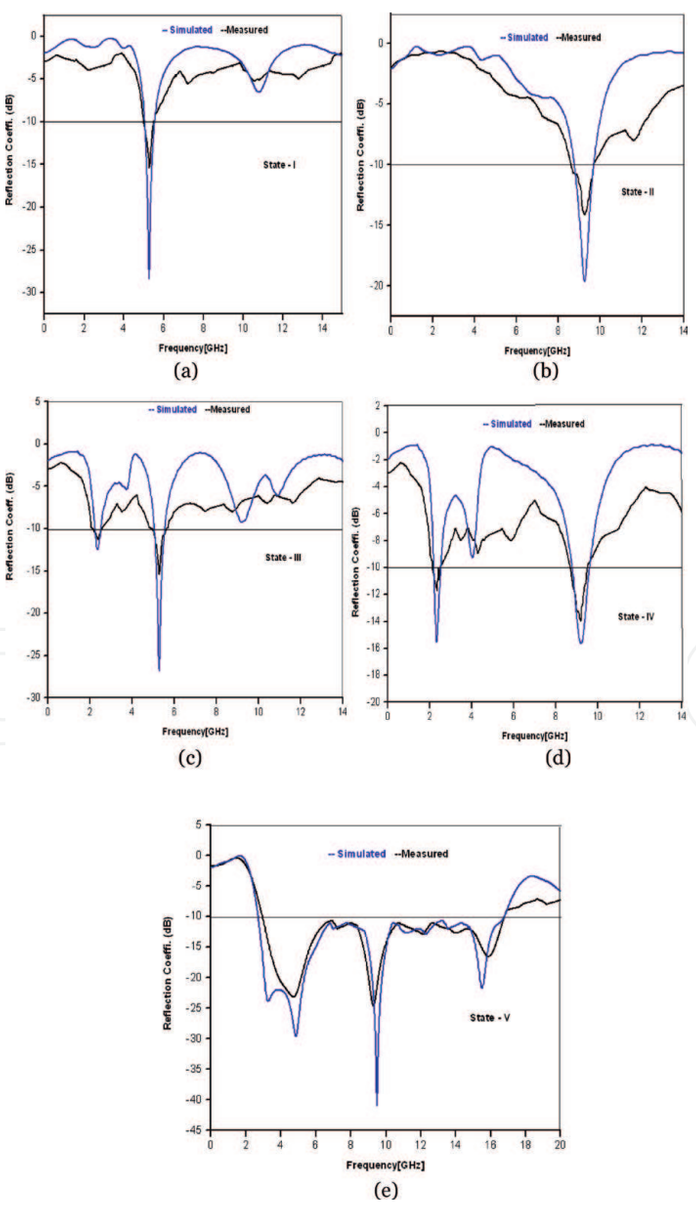

Figure 12.
Simulated and measured reflection coefficient S_{11} of the proposed antenna for states I-V (from (a)-(e) as per **Table 1***).*

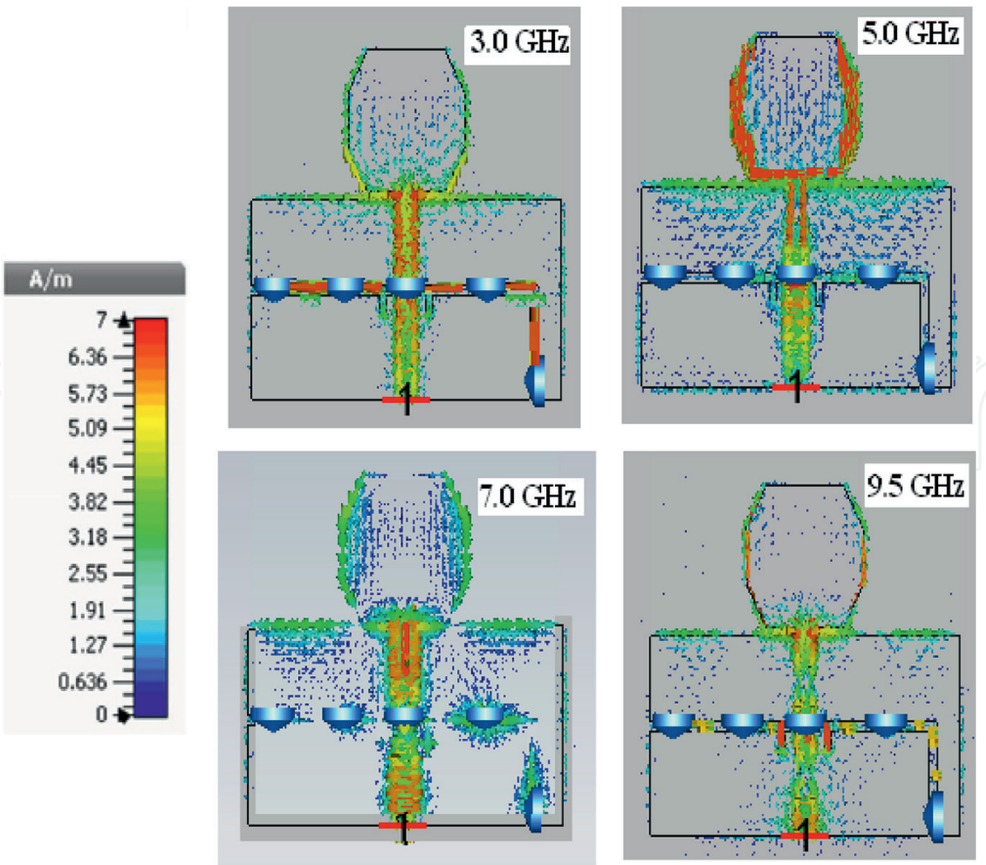

Figure 13.
Surface current distribution of the proposed antenna for different frequencies.

and 5.15–5.85 GHz and 3.1–10.6 GHz respectively. Proposed design also covers the airborne radar applications works at 9.2 GHz.

From **Figure 12(e)**, the resonance is identified at the frequency of 3.0, 5.0, 7.0 and 9.6 GHz. As per the observation of **Figure 13**, it is found that the first resonance is controlled by the inverted L shaped slot dimensions since the maximum surface current is present across it. Second resonance 5.0 GHz is obtained due to the octagonal shape of radiating element and the feedline attached to the patch. Third resonance at 7.0 GHz is obtained due to the rectangular slot created on the ground plane. The two rectangular slits dimensions of l_2 and W_2 are responsible to generate tank circuit causes the fourth resonance at 9.5 GHz. The surface current distribution is observed at theses resonance frequencies as shown in **Figure 13**.

From **Figure 14**, the 3D-gain of the antenna is observed at different resonant frequencies, where the maximum radiation is identify at the various values of angles (theta and phi). It is noticed that at higher frequency, the directivity is improved so that the gain is increased. **Figure 15** represents the measured antenna gain in single band, dual band and UWB modes for various switching states. It is analyzed that at lower frequency range gain is reduced whereas at higher frequencies (above 6 GHz) gain is improved as compared to reference gain level of 4 dB. It is also observed that antenna exhibit the acceptable gain in narrowband and dual-band modes. **Figure 15(b)** shows the average gain of 3.9 dB is achieved for UWB mode of the proposed antenna.

Figure 16(a) indicates the variation of the simulated radiation efficiency from 96.9 to 79.5% and from 97.2 to 70.3% for switching states I and II respectively, for the proposed antenna. The variation of the simulated radiation efficiency from 95.5 to 73.3% and from 94.0 to 78.1% is observed for state III and IV respectively. **Figure 16(b)** shows the simulated radiation efficiency variation from 98.9 to 85.8% for UWB

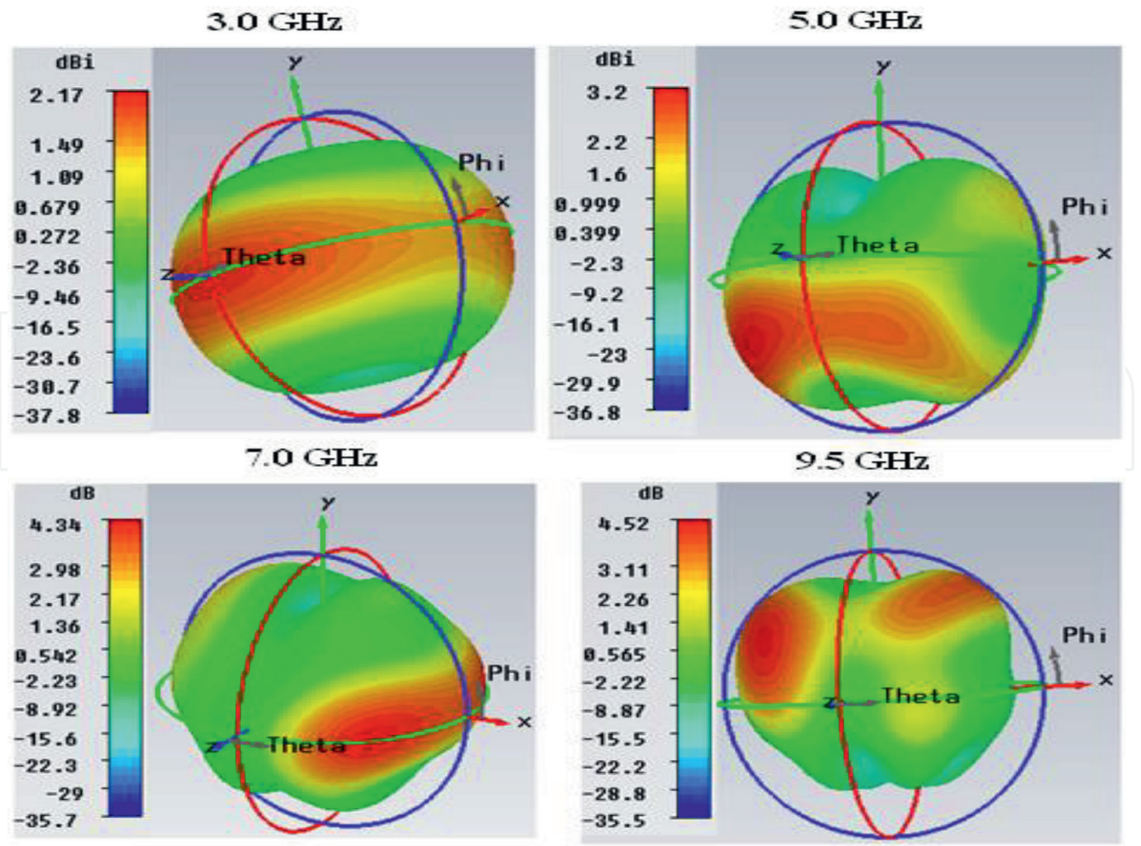

Figure 14.
Simulated gain (dB) of the proposed antenna for different frequencies.

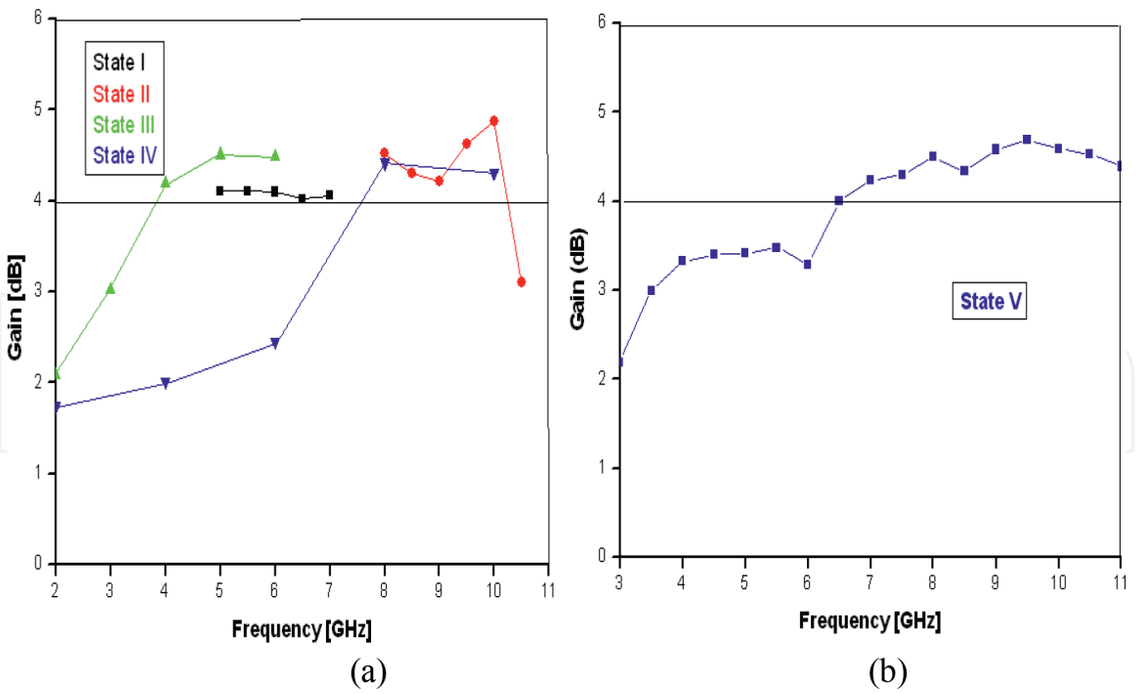

Figure 15.
Measured gain of the proposed antenna for different switching states: (a) single-band and dual-band modes and (b) UWB.

mode. It is noticed that the radiation efficiency is stay above the 70% in all the narrow band, dual band and UWB band. Another observation is that at higher frequency range the simulated radiation efficiency is decreases.

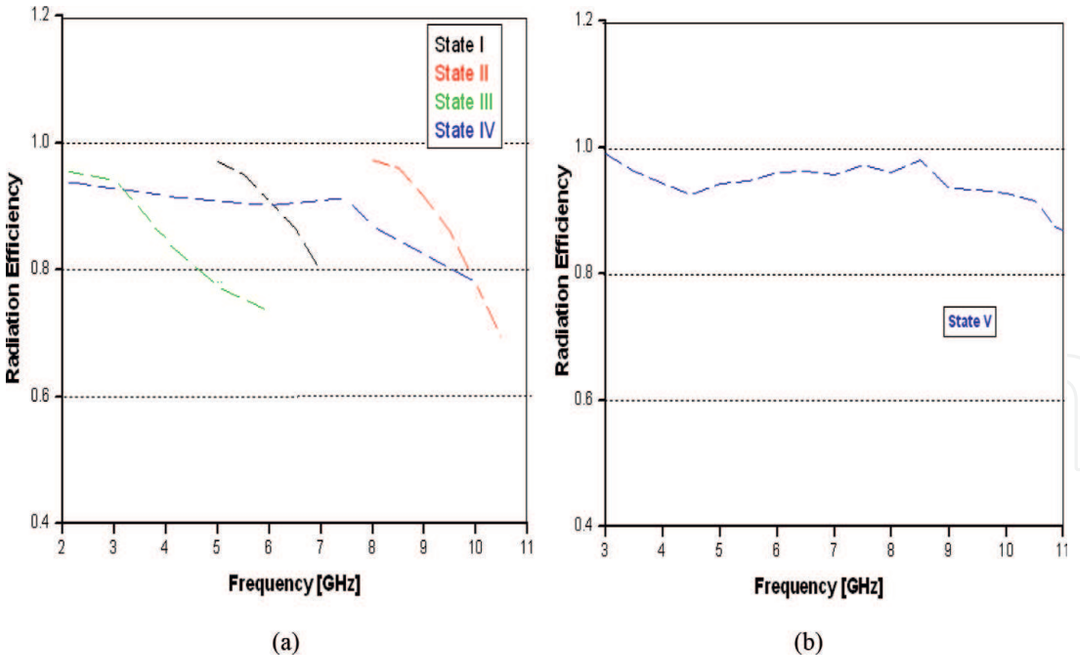

Figure 16.
Simulated radiation efficiency of the proposed antenna for different switching states: (a) single-band and dual-band modes and (b) UWB.

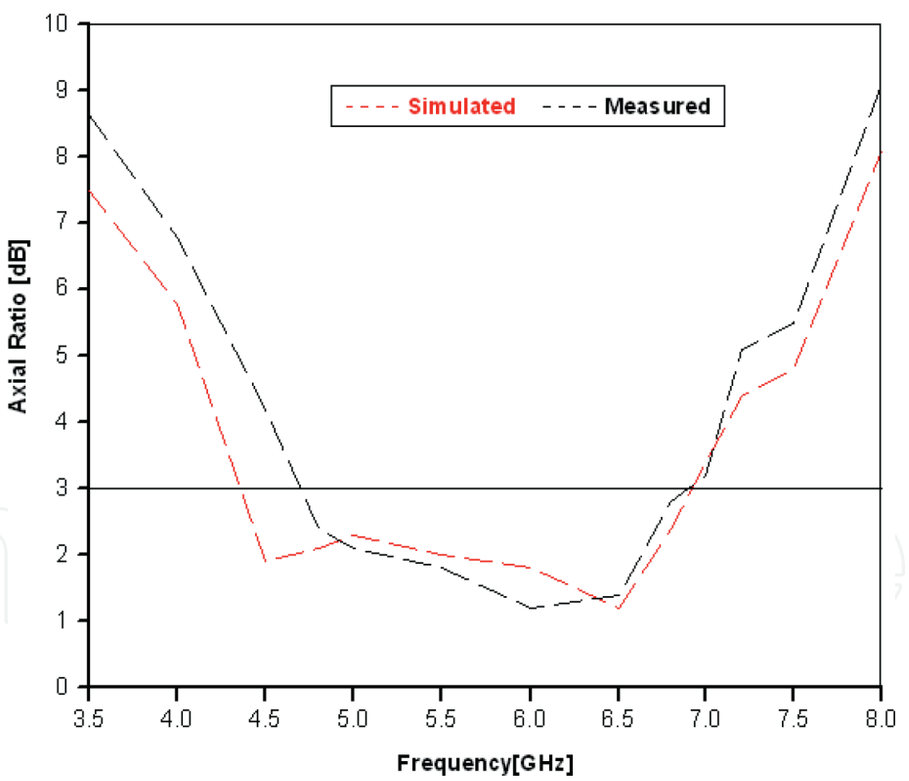

Figure 17.
Simulated and measured AR (axial ratio) (along $\theta = 78°$ and $\Phi = -89°$) of the proposed antenna.

The axial ratio (AR) measurement of the proposed antenna is done inside an anechoic chamber by using antenna measurement system with VNA. To obtain maximum ARBW (axial ratio bandwidth), the antenna measurement system is aligned along the directions of $\theta = 78°$ and $\Phi = -89°$, where AR is stay below the 3 dB reference level. The simulated ARBW of 38% is achieved for frequency range from 4.65 to 6.85 GHz as shown in **Figure 17**. The measured ARBW is slightly less than the simulated one at the center frequency 5.65 GHz.

Patterns are analyzed at operating frequencies 2.4, 5.4, 7.5, and 10 GHz for E and H plane (principal plane). From **Figure 18**, there is dumb bell shape and quasi-omnidirectional like radiation patterns in H-Plane and E-Plane respectively, which represents that the proposed design is a good candidate for wireless communication. There is a good agreement seen between the measured and simulated radiation patterns for E and H plane with the slight difference caused due to assembly

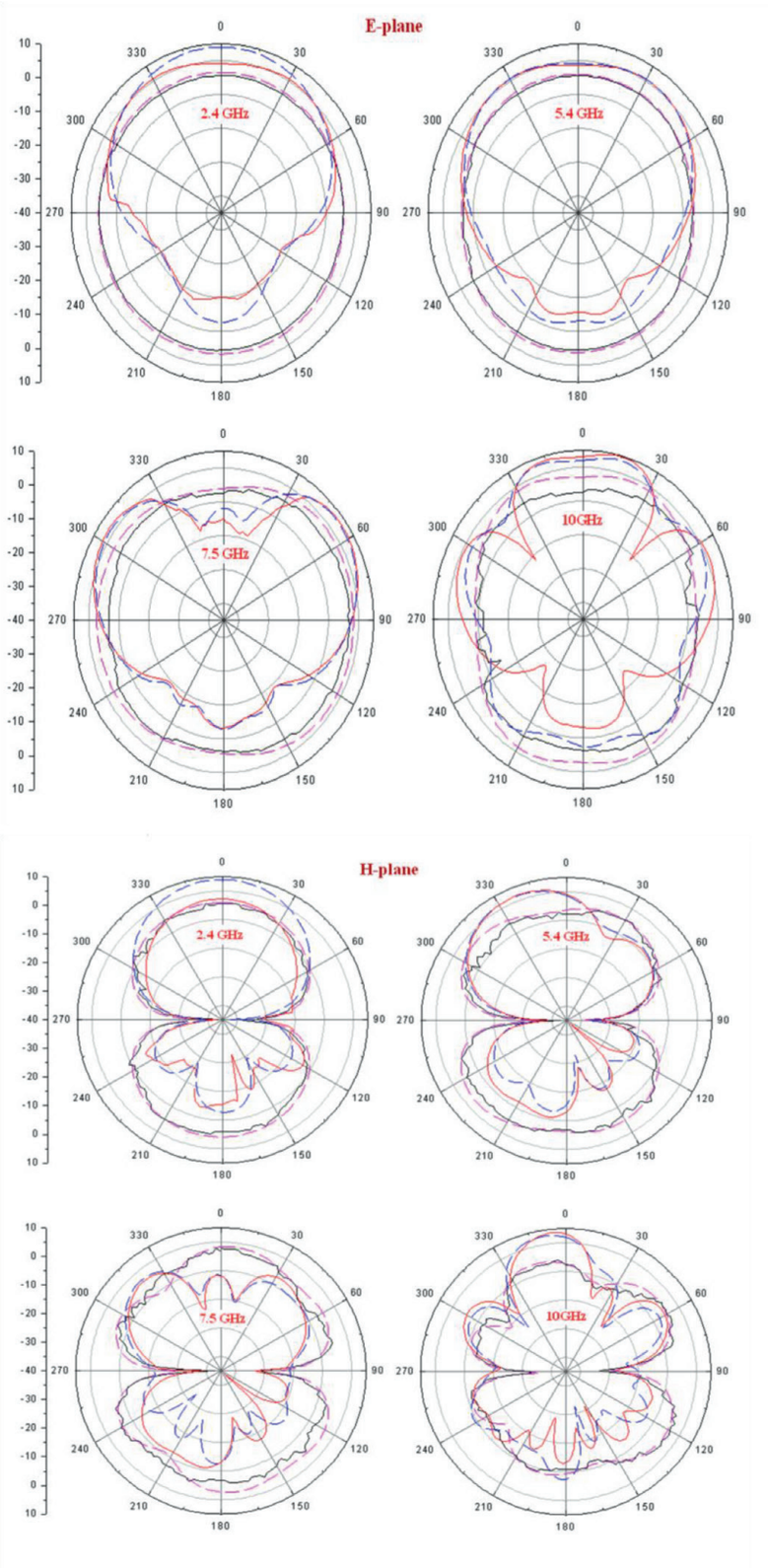

Figure 18.
Measured and simulated E and H plane radiation patterns.

Ref.	Year	Antenna size (in mm^3)	Bandwidth (in %)	Gain (in dBi)	Radiation efficiency (in %)	No. of operating modes (in GHz)	Covered wireless standards	Frequency Band Reconfigurability Achieved
Ref [17]	2013	49 × 49 × 6	2.63/3.28/6.44	4.93/2.85/5.12	89.9/91.8/97.6	3	GPS/WLAN/WiMAX (1.52/2.44/3.57)	No
Ref [20]	2013	52.6 × 30 × 1	47.27/38.88	−0.56/−0.62	89.2/98.1	2	GPS/WLAN (1.5/2.4)	No
Ref [21]	2014	40 × 40 × 1.6	34.48/18.28/19.96	3.97/4.04/3.25	—	3	(WLAN/WiMAX (2.4/3.5/5.8)	No
Ref [22]	2015	56 × 44 × 0.8	5.56/5.86/19.34/13.69	1.3/2.3/3.5/4.4	76.8/80.1/96.6/85.5	4	GPS/WLAN/WiMAX (1.5/2.4/3.5/5.4)	No
Ref [14]	2015	55 × 50 × 1.9	25.3/16.95/12.32	5.71/6.16/6.48	79/86.6/88.7	3	(WLAN/WiMAX (2.4/3.5/5.8)	No
Ref [23]	2016	48 × 48 × 1.6	20.73/15.02/31.96	1.64/2.07/4.06	66.2/77.15/87.6	3	GPS/WLAN (1.9/2.4/5)	No
Ref [15]	2017	40 × 40 × 1.6	1.9/14/5	−4.5/3.75/5.3	10/91/87	3	(GPS/WLAN/WiMAX (1.5/3.5/ 5.4)	No
Ref [24]	2017	50 × 50 × 1.6	2/12/18.2	6.35/5.57/3.9	82.1/84.9/90.9	3	(WLAN/ X Band) (4.8/5.8/9.2)	No
Ref [25]	2018	40 × 40 × 1.6	11.49/3.37/8.61	1.78/3.5/4.4	75.62/72/73	3	(WLAN/ WiMAX Band) (2.4/3.5/ 5.5)	No
Ref [26]	2018	30 × 24.8 × 1.6	3.5/5.01/13.2/5.77	1.35/1/1.07/1.75	—	4	(WiMAX/X Band) (3.1/5.52/7.31/9.72)	No
Proposed antenna		40 × 40 × 0.40	13/15/16/141/16/11	2.1/3.3/3.5/3.9/2.2/4.2	96.7/92.7/94.2/74.4/95.8/91.2	6	WLAN/WiMAX/WiFi/UWB/ ISM Band/Radar Application Band (2.4/5.2/5.8/3.1–10.6/2.45/9.2)	Yes

Table 2.
Comparison of propose designed with those in the state-of-art literature.

misalignments. A consistent omnidirectional radiation is observed in the E plane and a nearly bi-directional pattern is observed along the H plane for all the operating frequencies.

Both the measured and simulated E and H plane radiation patterns are appear reasonably stable with respect to resonant frequency. It is also observed that there is pinch-off along the end fire directions (θ = ±90°) at lower frequencies for H-plane pattern. The E-plane pattern shows the unidirectional nature at higher frequencies because at these frequencies the back lobes (along θ = 180°) are considerably decreases. **Table 2** shows the comparison of the proposed antenna characteristics, like as antenna size, impedance bandwidth, gain, radiation efficiency and operating modes, with reported multiband antennas for wireless standard.

5. Conclusion

A frequency band reconfigurable antenna suitable for WLAN (2.4/5.2 GHz). ISM band (2.4–2.5 GHz), WiMAX (2.3–2.4 and 5.15–5.85 GHz), WiFi (2.40–2.48 and 5.15–5.85 GHz) and UWB (3.1–10.6 GHz) wireless standards are presented in this chapter. Proposed design also covers the airborne radar applications works at 9.2 GHz. The radiating element of octagonal shape and switchable slotted ground is implemented to achieve the frequency band reconfigurability between wireless standards. The switching between the narrowband, dual band and UWB modes is obtain by using five p-i-n diodes placed inside the inverted L shaped ground slot. The proposed design is provides the facility of easily integration with cognitive radio and multi radio wireless terminal devices. Proposed design achieve the bandwidth of 16% (5.05–5.89 GHz) and 14% (5.01–5.79 GHz) in simulation and measurement mode respectively for narrowband states I. Next it obtained bandwidth of 11% (8.76–9.80 GHz) and 10% (8.68–9.69 GHz) in simulation and measurement mode respectively for narrowband states II. Antenna resonant in dual band mode and achieve impedance bandwidth of 13% (2.21–2.52 GHz) and 15% (5.07–5.89 GHz) under simulation and 12% (2.20–2.50 GHz) and 15% (5.05–5.90 GHz) during measurement for next state III. For next state IV, antenna identifies the operating bandwidth of 14% (2.18–2.52 GHz) and 10% (8.78–9.71 GHz) and 13% (2.19–2.50 GHz) and 9% (8.70–9.60 GHz) during simulation and measurement mode respectively. For UWB mode of V state, antenna indicate the operating bandwidth of 141% (2.87–16.87 GHz) and 140% (2.97–16.80 GHz) under simulation and measurement mode respectively. The average gain of 3.9 dB is achieved for UWB mode of the proposed antenna. The radiation efficiency is stay above the 70% in all the narrow band, dual band and UWB band. Radiation characteristics of the proposed antenna are achieved with good impedance matching at these resonant frequencies. The radiation pattern, gain and efficiency are consistent over all the operating bands making the proposed antenna a good choice for wireless applications.

Conflict of interest

The author(s) declare(s) that there is no conflict of interest regarding the publication of this paper.

Author details

Ritesh Kumar Saraswat[1*] and Mithilesh Kumar[2]

1 M.L.V. Govt. Textile and Engineering College, Bhilwara, Rajasthan, India

2 Rajasthan Technical University, Kota, Rajasthan, India

*Address all correspondence to: ritesh.saraswat9@gmail.com

References

[1] Zhang C, Yang S, Pan HK, Fathy AE, Nair VK. Frequency reconfigurable antennas for multi radio wireless platforms. IEEE Microwave Magazine. 2009;**10**(1):66-83. DOI: 10.1109/MMM.2008.930677

[2] FCC (Federal Communications Commission). First Report and order. 2002

[3] Li RL, Wu T, Eom SY, Myoung SS, Lim K, Laskar J, et al. Switchable quad-band antennas for cognitive radio base station applications. IEEE Transactions on Antennas and Propagation. 2010;**58**(5):1468-1476. DOI: 10.1109/TAP.2010.2044472

[4] Mahmoud SF, Sheta AF. A widely tunable compact patch antenna. IEEE Antennas and Wireless Propagation Letters. 2008;**7**:40-42. DOI: 10.1109/LAWP.2008.915796

[5] Huang CT, Han TY. Reconfigurable monopolar patch antenna. Electronics Letters. 2010;**46**(3):199-200. DOI: 10.1049/el.2010.3242

[6] Gardner P, Hamid MR, Hall PS, Ghanem F. Switched-band Vivaldi antenna. IEEE Transactions on Antennas and Propagation. 2011;**59**(5):1472-1480. DOI: 10.1109/TAP.2011.2122293

[7] Li RL, Jin GP, Zhang DL. Optically controlled reconfigurable antenna for cognitive radio applications. Electronics Letters. 2011;**47**(17):948-950. DOI: 10.1049/el.2011.1958

[8] Gardner P, Hamid MR, Hall PS, Ghanem F. Vivaldi antenna with integrated switchable band pass resonator. IEEE Transactions on Antennas and Propagation. 2011;**59**(11):4008-4015. DOI: 10.1109/TAP.2011.2164197

[9] Ghafouri-Shiraz H, Tariq A. Frequency-reconfigurable monopole antennas. IEEE Transactions on Antennas and Propagation. 2012;**60**(1):44-50. DOI: 10.1109/TAP.2011.2167929

[10] Gardner P, Kelly JR, Hall PS. Integrated wide-narrow band antenna for switched operation. In: Processing IEEE EuCAP; 2009; Berlin, Germany. 2009. pp. 3757-3760

[11] Boudaghi H, Azarmanesh M, Mehranpour M. A frequency-reconfigurable monopole antenna using switchable slotted ground structure. IEEE Antennas and Wireless Propagation Letters. 2012;**11**:655-658. DOI: 10.1109/LAWP.2012.2204030

[12] Thalakotuna D, Matekovits L, Heimlich M, Esselle KP, Hay SG. Active switching devices in a tunable EBG structure: Placement strategies and modeling. Journal of Electromagnetic Waves and Applications. 2011;**25**(11):1740-1751. DOI: 10.1163/156939311797164873

[13] Thalakotuna DNP, Esselle KP, Matekovits L, Heimlich M, Hay SG. Changing the electromagnetic bandgap and stopbands in a multistate periodic circuit. Microwave and Optical Technology Letters. 2013;**55**(8):1871-1874. DOI: 10.1002/mop.27675

[14] Ahsan MR, Islam M, Ullah MH. Computational and experimental analysis of high gain antenna for WLAN/WiMAX applications. Journal of Computational Electronics. 2015;**14**(2):634-641. DOI: 10.1007/s10825-015-0699-8

[15] Rajabloo H, Kooshki VA, Oraizi H. Compact microstrip fractal Koch slot antenna with ELC coupling load for triple band application. AEU-International Journal of Electronics and Communications. 2017;**73**:144-149. DOI: 10.1016/j.aeue.2016.12.027

[16] Ali T, Fatima N, Biradara RC. Miniaturized multiband reconfigurable fractal slot antenna for GPS/GNSS/Bluetooth/WiMAX/X-band applications. AEU-International Journal of Electronics and Communications. 2018;**94**:234-243. DOI: 10.1016/j.aeue.2018.07.017

[17] Xu HX, Wang GM, Qi MQ. A miniaturized triple-band metamaterial antenna with radiation pattern selectivity and polarization diversity. Progress in Electromagnetics Research. 2013;**137**:275-292. DOI: 10.2528/PIER12081008

[18] Saraswat RK, Kumar M. Miniaturized slotted ground UWB antenna loaded with metamaterial for WLAN and WiMAX applications. Progress in Electromagnetics Research B. 2016;**65**:65-80. DOI: 10.2528/PIERB15112703

[19] Rahimi M, Zarrabi FB, Ahmadian R, Mansouri Z, Keshtkar A. Miniaturization of antenna for wireless application with difference metamaterial structures. Progress in Electromagnetics Research. 2014;**145**:19-29. DOI: 10.2528/PIER13120902

[20] Xu HX, Wang GM, Lv YY, Qi MQ, Gao X, Ge S. Multi frequency monopole antennas by loading metamaterial transmission lines with dual-shunt branch circuit. Progress in Electromagnetics Research. 2013;**137**:703-725. DOI: 10.2528/PIER12122409

[21] Samsuzzaman M, Islam T, Abd Rahman NH, MRI F, Mandeep JS. Compact modified swastika shape patch antenna for WLAN/WiMAX applications. International Journal of Antennas and Propagation. 2014;**2014**: 1-8. DOI: 10.1155/2014/825697

[22] Cao YF, Cheung SW, Yuk TI. A multiband slot antenna for GPS/WiMAX/WLAN systems. IEEE Transactions on Antennas and Propagation. 2015;**63**(3):952-958. DOI: 10.1109/TAP.2015.2389219

[23] Alam T, Samsuzzaman M, Faruque MRI, Islam MT. A metamaterial unit cell inspired antenna for mobile wireless applications. Microwave and Optical Technology Letters. 2016;**58**(2):263-267. DOI: 10.1002/mop.29543

[24] Vinodha E, Raghavan S. Double stub microstrip fed two element rectangular dielectric resonator antenna for multiband operation. AEU-International Journal of Electronics and Communications. 2017;**78**:46-53. DOI: 10.1016/j.aeue.2017.05.020

[25] Varamini G, Keshtkar A, Naser-Moghadasi M. Compact and miniaturized microstrip antenna based on fractal and metamaterial loads with reconfigurable qualification. AEU-International Journal of Electronics and Communications. 2018;**83**:213-221. DOI: 10.1016/j.aeue.2017.08.057

[26] Ali T, Saadh M, Biradar RC. A fractal quad-band antenna loaded with L-shaped slot and metamaterial for wireless applications. International Journal of Microwave and Wireless Technologies. 2018;**10**(7):826-834. DOI: 10.1017/S1759078718000272

[27] Computer Simulation Technology–CST (Microwave Studio MWS). Version-2014

[28] Alpha Industries. ALPHA-6355 beamlead PIN diode. Data sheet [Online]. 2015. Available from: http://www.datasheetarchive.com/ALPHA/PINdiode6355-datasheet.html